

pubs.acs.org/acsaom Article

# Luminescent Cyclometalated Platinum Acyclic Diaminocarbene Complexes as PhOLED Dopants

Yennie H. Nguyen,<sup>#</sup> Linh T. M. Dang,<sup>#</sup> Marjolaine Cornu,<sup>#</sup> Chenggang Jiang, Allana C. Darrow, Vinh Q. Dang, and Thomas S. Teets\*



Cite This: ACS Appl. Opt. Mater. 2024, 2, 2019-2030



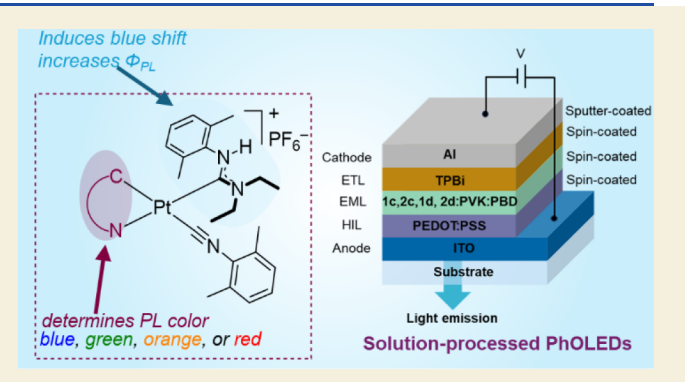
**ACCESS** I

III Metrics & More

Article Recommendations

s Supporting Information

**ABSTRACT:** There is continuing demand for the discovery of phosphorescent organometallic complexes for applications in phosphorescent organic light-emitting diodes (PhOLEDs), one of the most efficient and well-developed color display technologies. This study explores a class of phosphorescent cationic cyclometalated platinum complexes, using a range of cyclometalating (C^N) ligands paired with 2,6-dimethyphenyl isocyanide (CN<sup>dmp</sup>) and acyclic diaminocarbene (ADC) ligands. The compounds are prepared via a two-step procedure. The intermediate bis-isocyanide complexes, with the general formula  $[Pt(C^N)(CN^{dmp})_2](PF_6)$ , are converted to the final mixed ADC/isocyanide compounds,  $[Pt(C^N)(ADC)(CN^{dmp})](PF_6)$ , by nucleophilic addition of diethylamine to one of the isocyanides. Structural characterization



by single-crystal X-ray diffraction reveals that the isocyanide *trans* to the neutral N-heterocycle of the C^N ligand is always the one converted to an ADC. Conversion of one isocyanide into an ADC brings about notable shifts in redox potentials and the gap between the highest occupied molecular orbital (HOMO) and the lowest unoccupied molecular orbital (LUMO). Photophysical studies reveal that the ADC compounds have blue-shifted photoluminescence relative to the isocyanide precursors, with higher photoluminescence quantum yields and longer lifetimes, particularly for complexes emitting in the blue region. Solution-processed PhOLEDs using two of the best-performing bis-isocyanide and ADC platinum complexes as the emitters were successfully fabricated and display sky-blue electroluminescence (EL).

KEYWORDS: cyclometalated, platinum, phosphorescence, carbenes, OLED

#### **■** INTRODUCTION

Phosphorescent organic light-emitting diode (PhOLED) devices represent a significant advancement in OLED technology, offering higher efficiency and longer device lifetimes compared to fluorescent OLEDs. The use of phosphorescent dopants allows these devices to achieve nearly 100% internal efficiency. Solution-processed PhOLEDs are increasingly preferred over vacuum-processed PhOLEDs due to their cost-effectiveness, ability to cover larger areas, and flexibility in production methods. This technology shows significant potential for applications like mobile displays, monitors, and televisions, promising enhanced performance and manufacturing versatility for next-generation OLED devices. 4-7

Cyclometalated platinum complexes are recognized as a promising material for PhOLED applications, thanks to their high luminescence quantum yields, relatively short phosphorescence lifetimes, and straightforward color tuning capabilities. The photoluminescence (PL) profiles of these platinum complexes are most readily tuned by modifying the cyclometalating ligand, with the other supporting ligands (ancillary

ligands) playing a secondary role. Like other 5d phosphorescent emitters, high photoluminescence quantum yields are possible, in part due to platinum's considerable ligand-field strength, which increases the energy of nonradiative metal-centered ( $^3MC$ ) d-d states and, in most cases, effectively prevents thermal population of these states.  $^{8-15}$ 

An emerging category of cyclometalated platinum complexes features isocyanide and/or acyclic diaminocarbene (ADC) ancillary ligands. These mainly include charge-neutral chloride terminated complexes with one isocyanide <sup>16–19</sup> or ADC, <sup>20</sup> and a recent study used compounds from these categories as PhOLED dopants, while also introducing cationic bisisocyanide and bis-ADC cyclometalated platinum complexes for the same application. <sup>21</sup> Our group has demonstrated that

Received: August 7, 2024
Revised: September 6, 2024
Accepted: September 9, 2024
Published: September 18, 2024





acyclic diaminocarbene (ADC) ancillary ligands can substantially increase the PL quantum yields and lifetimes in platinum acetylide  $^{22-25}$  and cyclometalated platinum complexes,  $^{26}$  and there are also several other examples of luminescent complexes of other metals ( $M=\mathrm{Pd}$ , Re, and Ir) supported by ADCs.  $^{14,27-31}$  Most of the above-mentioned previous studies on ADC-supported cyclometalated platinum complexes focused on phosphorescence in the blue to green regions, and only one involved PhOLED applications.  $^{21}$  Thus, an unanswered question is whether ADC ligands can have profound effects on the photoluminescence and/or excited-state dynamics in other classes of cyclometalated platinum compounds with PL outside of the blue region, and the extent to which these next-generation compounds can function as PhOLED dopants.

In this study, we describe a new class of cyclometalated platinum complexes supported by ADCs, spanning a range of luminescence colors from blue to red. The cationic complexes have a mixed ancillary ligand set consisting of one isocyanide and one ADC (Figure 1). The cyclometalating ligands we

**Figure 1.** Platinum mono-ADC complexes with various C^N ligands to produce different luminescence colors.

employ (see Figure 1) are 1-phenylisoquinoline (piq, red PL), 2-phenylquinoline (pq, orange PL), 2-phenylpyridine (ppy, green PL), 2-(2,4-difluorophenyl)pyridine) (F<sub>2</sub>ppy, sky blue PL) and 1-phenylpyrazole (ppz, blue PL). The ADC-

supported cyclometalated Pt complexes are synthesized via a two-step process starting with the  $[Pt(C^N)(\mu-Cl)]_2$  dimers. Photophysical studies show that the ADC donor induces a blueshift in PL in all cases, relative to analogous isocyanide complexes, which is particularly pronounced in the higherenergy green to blue emitters bearing ppy, F2ppy, and ppz cyclometalating ligands. The photoluminescence quantum yields are enhanced by a factor of 1.2 to 2.7 relative to the isocyanide precursor, again with the most significant increase observed in one of the blue-phosphorescent compounds with  $C^N = F_2ppy$ . Taken together, these results underscore the ability of ADCs to both tune the PL color and enhance the quantum yields of photoluminescent platinum complexes with a wide range of color profiles. Lastly, four of the cyclometalated platinum complexes (two bis-isocyanide complexes and two ADC complexes) with  $C^N = ppy$  or  $F_2ppy$  are employed as emissive dopants in solution-processed PhOLEDs, resulting in sky-blue electroluminescence (EL) output.

## ■ RESULTS AND DISCUSSION

### **Synthesis and Structural Characterization**

The procedure for synthesizing the new class of ADCsupported cyclometalated platinum complexes is outlined in Scheme 1. Bis-isocyanide platinum complexes 1a-e are prepared by treating their chloro-bridged dimer precursors with 2 equiv of 2,6-dimethylphenyl isocyanide and silver hexafluorophosphate in dichloromethane, under a nitrogen atmosphere at room temperature overnight. After completion, the reaction mixtures were filtered through Celite to remove AgCl, followed by reducing the solvent volume under vacuum and crystallizing the product by adding pentane and diethyl ether. The resulting precipitates were filtered, washed with pentane or diethyl ether, and vacuum-dried overnight, yielding the desired products with moderate to good overall yields ranging from 52% to 83%, with the exception of the piq analogue (1a), which was obtained in a lower yield of 30%. Subsequently, nucleophilic addition of diethylamine yielded ADC complexes 2a-e, achieved by introducing excess diethylamine to the isocyanide precursor in dichloromethane at room temperature. NMR spectra of crude products indicated minor, unidentifiable aromatic impurities, necessitating additional purification via recrystallization to ensure there

Scheme 1. Synthesis of New Mono ADC Platinum C^N Complexes

were no luminescent impurities present. The desired products were isolated in yields ranging from low to moderate, specifically 24% to 36%, mainly due to product loss during recrystallization. NMR spectra (Figures S2-S21) are consistent with the proposed structures. Moreover, infrared (IR) spectroscopy (Figures S22-S31) is valuable for illustrating structural differences between the bis-isocyanide complexes (1a-e) and the product ADC complexes (2a-e). In all cases, a single  $\tilde{\nu}_{C\equiv N}$  stretching frequency, originating from the isocyanide ligand(s), is observed. The observed frequency is always lower in the ADC complexes, by 7-27 cm<sup>-1</sup> relative to the respective bis-isocyanide precursor, consistent with the ADC donating more electron density to the platinum center and increasing  $\pi$  backbonding to the isocyanide. In addition, the ADC complexes exhibit a sharp  $\tilde{\nu}_{\mathrm{N-H}}$  peak at a frequency of 3345-3363 cm<sup>-1</sup>, which is absent in the bis-isocyanide complexes and signifies the formation of the ADC.

All the compounds except 1d were further characterized by single-crystal X-ray diffraction, and the refinement data are summarized in Tables S1—S4. In the case of the bis-isocyanide complexes 1, molecular structures for 1a and 1e are shown in Figure 2 as representative examples, with the remaining bis-

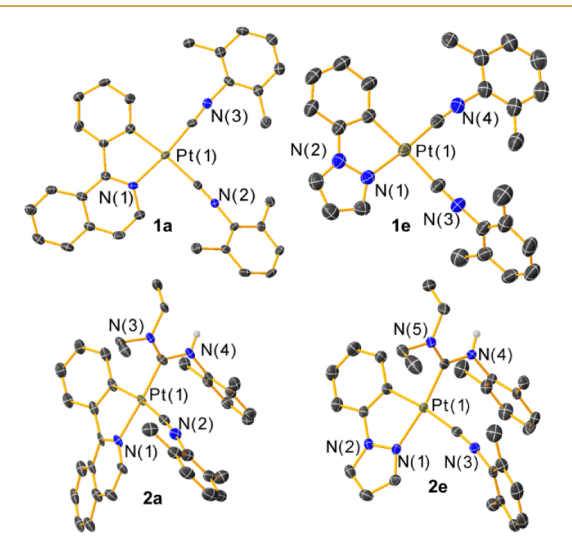


**Figure 2.** Molecular structures of platinum complexes **1a**, **1e**, **2a**, and **2e**, determined by single-crystal X-ray diffraction. Diffraction data were collected at 123 K for all compounds except **1e**, which was measured at 298 K. Ellipsoids are shown at 50% probability level for **1a**, **2a**, and **2e**. The higher data collection temperature for **1e** led to larger thermal displacement, so the ellipsoids are plotted at 30% probability level for that structure. All the hydrogen atoms, PF<sub>6</sub><sup>-</sup> counterions, and solvent molecules are omitted for clarity.

isocyanide structures shown in Figures S32 and S33. The sum of the bond angles around Pt center is close to 360° in all cases, consistent with the planar coordination geometry. The isocyanides *trans* to the *N*-heterocycle ring have a slightly shorter Pt–C bond length in the range of 1.918(4)–1.930(4) Å, while the Pt–C bond distance for the isocyanide *trans* to the metalated aryl ring span 1.999(6) Å to 2.037(5) Å, consistent with the stronger *trans* influence of the aryl group. These observed isocyanide Pt–C bond distances are similar to those of other Pt(II) isocyanide complexes reported in the literature. <sup>22,23,25,26</sup>

For the platinum ADC compounds, the structures of compounds 2a and 2e are depicted in Figure 2, while those

for **2b**, **2c**, and **2d** are available in Figures S34–S36. The coordination geometry around the Pt center remains approximately planar in **2a–e**, with the ADC ancillary ligand arranged *trans* to the *N*-heterocycle of the cyclometalating ligand. In all cases, the ADC ligand is nearly perpendicular to the coordination plane to avoid steric clash with all the other ligands. The Pt– $C_{\rm ADC}$  bond distances span in a narrow range of 1.995(3)–2.009(3) Å, slightly longer than the corresponding isocyanide Pt–C distance in the bis-isocyanide complexes (1a–c and 1e, see above), most likely due to more significant  $\pi$ –backbonding in the isocyanide as compared to the ADC ligand.

#### Electrochemistry

To assess the impact of the cyclometalating ligands and ADCs on redox potentials and relative frontier orbital energies, cyclic voltammograms were conducted on both isocyanide complexes 1a-1e and ADC complexes 2a-2e, as illustrated in Figure 3.

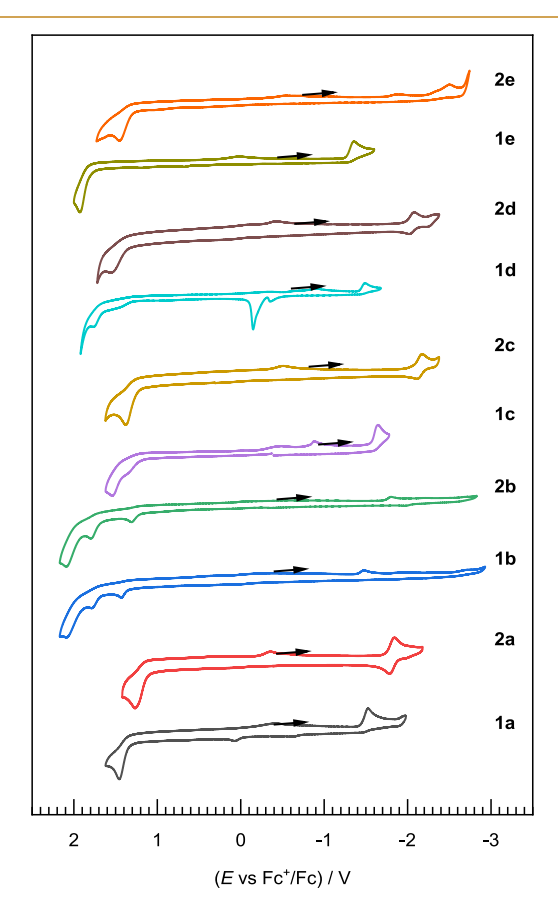


**Figure 3.** Overlaid cyclic voltammograms of **1a-e** and **2a-e** in acetonitrile with 0.1 M TBAPF<sub>6</sub> supporting electrolyte, a glassy carbon working electrode, and a scan rate of 0.1 V/s. Currents are normalized to bring all the traces onto the same scale for better comparison. The potential was referenced to an internal standard of ferrocene.

Notably, all complexes feature a reduction wave that is quasireversible in some cases and irreversible in others, and two irreversible oxidation events. Therefore, we employed a method endorsed by the Vullev group to estimate the thermodynamic potential from irreversible couples,<sup>32</sup> with half-peak potentials reported in Table 1. The reduction potentials ( $E^{\text{red}}$ ) of the ADC complexes exhibit a notable cathodic shift toward more negative values in comparison to

Table 1. Summary of Cyclic Voltammetry Data

	$(E \text{ vs } Fc^+/Fc)/V^a$		$E^{b}$ ,		
Complex	$E^{\text{ox}}\left([\text{Pt}]^{2+\bullet}/[\text{Pt}]^+\right)$	$E^{\mathrm{red}}$ ([Pt]+/[Pt]•)	НОМО	LUMO	$\Delta E_{\mathrm{H-L}}/\mathrm{eV}^c$
1a	1.40	-1.48	-6.20	-3.32	2.88
2a	1.18	-1.81	-5.98	-2.99	2.99
1b	1.39	-1.43	-6.19	-3.37	2.82
2b	1.25	-1.76	-6.05	-3.04	3.01
1c	1.40	-1.60	-6.20	-3.20	3.00
2c	1.31	-2.14	-6.11	-2.66	3.45
1d	1.66	-1.45	-6.46	-3.35	3.11
2d	1.43	-2.05	-6.23	-2.75	3.48
1e	1.86	-1.29	-6.66	-3.51	3.15
2e	1.36	-2.29	-6.16	-2.51	3.65

<sup>a</sup>All redox potentials are irreversible. Potentials are reported as half-peak potentials, i.e., the potential at which current reaches half of its maximum value for that wave. <sup>32</sup> [Pt]<sup>+</sup> indicates the initial closed-shell redox state of the cationic platinum complexes. <sup>b</sup>Absolute frontier orbital energies, estimated from equation  $E = -[(E \ vs \ Fc^+/Fc) + 4.8]$  using  $E^{ox}$  (HOMO) and the first  $E^{red}$  (LUMO). <sup>34</sup> <sup>c</sup>The energy difference between the HOMO and LUMO, i.e., the HOMO–LUMO gap.

their isocyanide precursors. Conversely, smaller shifts in the same direction were observed for the potentials corresponding to one-electron oxidation ( $E^{ox}$ ). These shifts are consistent with an ADC being more electron-rich than an isocyanide, making the compounds easier to oxidize and harder to reduce. Electrochemical HOMO-LUMO gaps were estimated from the CV data by taking the difference between the first reduction and first oxidation potentials and are also collected in Table 1. Converting isocyanides into ADCs consistently widened the HOMO-LUMO gap in all cases. We observe that the ADC destabilizes both the HOMO and LUMO, but this effect is notably pronounced in the LUMO. As is wellestablished for complexes with C^N cyclometalating ligands, the LUMO is a  $\pi^*$  orbital mostly localized on the Nheterocycle ring of the C^N ligand, while the HOMO tends to be more delocalized with significant contribution from the C^N aryl ring and the metal center. 15,33 We propose that because of their trans arrangement the N-heterocycle and isocyanide in la-e are conjugated and the LUMO is delocalized over the N-heterocycle  $\pi^*$  orbital and one of the isocyanide's  $C \equiv N \pi^*$  orbitals, leading to some stabilization of the LUMO. A similar conjugation effect involving isocyanides was observed in isocyanide-supported platinum acetylide complexes.<sup>22,23</sup> When the isocyanide is converted into an ADC in 2a-e, the ADC aligns perpendicular to the coordination plane and the single unoccupied  $2p\pi$  orbital on the ADC is thus perpendicular to the N-heterocycle's  $\pi^*$ LUMO, disrupting the conjugation and thus destabilizing the LUMO.

## **Photophysical Properties**

The UV–vis absorption spectra of complexes  ${\bf 1a-e}$  and  ${\bf 2a-e}$ , recorded in a  ${\rm CH_2Cl_2}$  solution, are shown in Figures 4 and 5, respectively (black traces). All compounds display strong absorption in the  $\lambda$  < 300 nm region, with less intense bands observed around 300–425 nm. Based on previous literature,  $^{4,5}$  the high-energy absorption bands, in the range of 250–300 nm, are mainly assigned to  $\pi \to \pi^*$  transitions located on the metalated C^N ligand. Less intense bands observed around 300–425 nm correspond to mixed intraligand ( $^1$ IL)/metal–to–ligand charge transfer ( $^1$ MLCT) transitions. The energies of the less intense absorption bands depend on the C^N ligand and follow the trend  ${\bf 1a/2a}$  (C^N = piq) <  ${\bf 1b/2b}$  (C^N = pq) <  ${\bf 1c/2c}$  (C^N = ppy) <  ${\bf 1d/2d}$  (C^N = F2ppy) <  ${\bf 1e/2e}$  (C^N

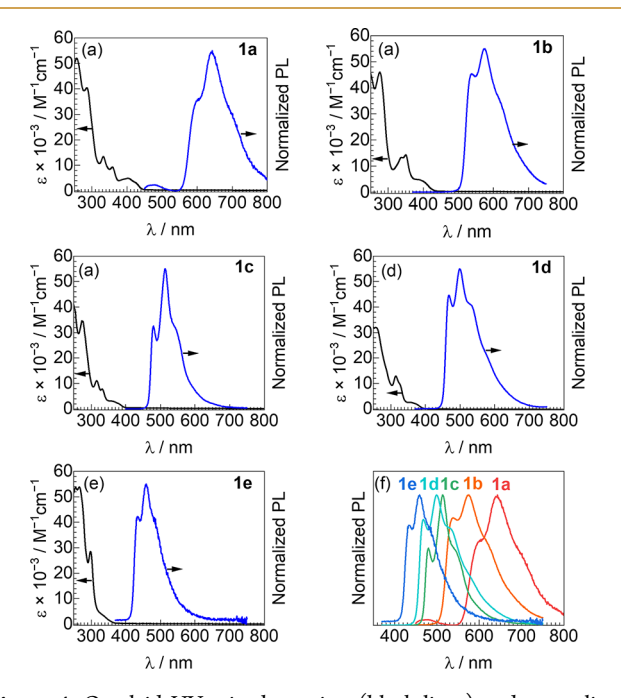


**Figure 4.** Overlaid UV—vis absorption (black lines) and normalized photoluminescence spectra (blue lines) of (a) 1a, (b) 1b, (c) 1c, (d) 1d, and (e) 1e. In (f), the same PL spectra are overlaid. Absorption spectra were recorded in  $CH_2Cl_2$  at room temperature, and PL spectra were recorded at 2 wt % in PMMA films at room-temperature.

= ppz), which correlates with the HOMO–LUMO gaps. When the ADC is introduced, the molar absorption coefficient of the most intense band decreases due to reduced conjugation in the complex, and there is a blue shift in the lower-energy band; this blueshift is consistent with the destabilization of the LUMO and increase in HOMO–LUMO gap in the ADC complexes, inferred above from CV measurements.

Photoluminescence spectra at 2 wt % in poly (methyl methacrylate) (PMMA) films are also shown in Figures 4 and 5 (blue lines). A summary of the photoluminescence properties of all complexes, including PL lifetimes, quantum yields, and calculated decay rates, are in Table 2. The PL profile and peak wavelength are primarily determined by the C^N ligand and correlate reasonably well with the HOMO–LUMO gap (Table 1). For a given series of compounds (1a–e or 2a–e), the peak PL wavelengths fall in the order C^N = ppz

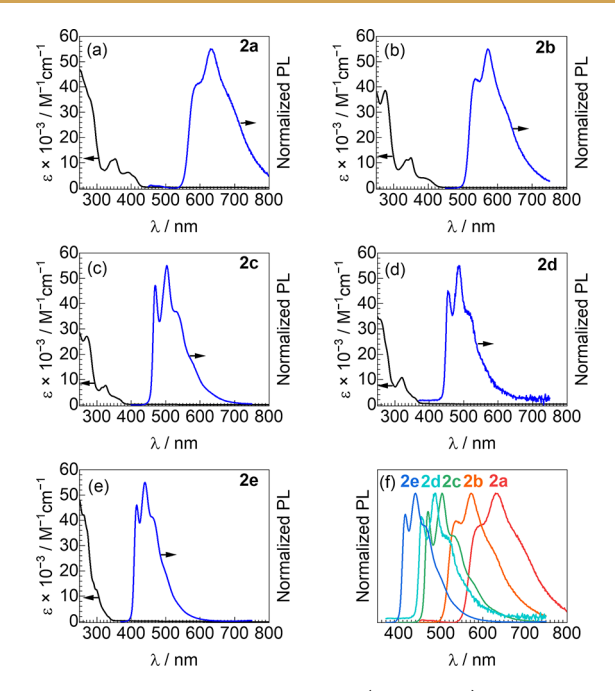


**Figure 5.** Overlaid UV—vis absorption (black lines) and normalized photoluminescence spectra (blue lines) of (a) 2a, (b) 2b, (c) 2c, (d) 2d, and (e) 2e. In (f), the same PL spectra are overlaid. Absorption spectra were recorded in  $CH_2Cl_2$  at room temperature, and PL spectra were recorded at 2 wt % in PMMA films at room-temperature.

<  $F_2ppy$  < ppy < pq < piq, and in all cases  $\lambda_{0-1}$  has the maximum intensity. To better visualize the effects of the C^N ligands on the PL profiles, Figures 4f and 5f overlay the spectra for each respective series of compounds. Replacing an isocyanide ligand with an ADC in complexes 1a-1e to form 2a-2e leads to a modest blue shift in their photoluminescence spectra, more clearly visualized in Figures S37-S41. The shift in  $\lambda_{0-0}$  is minimal when C^N = pq, with 1b and 2b only differing by 2 nm (69 cm<sup>-1</sup>), but more substantial hypsochromic shifts occur in the others when converting an isocyanide to an ADC, ranging from 9-19 nm (250-1000 cm-1). Again, these results are consistent with the CV experiments described above, where converting an isocyanide (1a-1e) to an ADC (2a-e) increases the HOMO-LUMO gap, at parity of C^N ligand. Moreover, as shown in Figures S42 and S43, there are no shifts or new features in the PL excitation spectra and the emission spectra in the 2 wt % PMMA films vs those in CH<sub>2</sub>Cl<sub>2</sub> solutions for each complex,

indicating there are no observed photophysical signatures attributed to aggregation in the films.

In PMMA films at 2 wt %, the photoluminescence quantum yields of complexes 1a-e range from 0.06 to 0.33. Introducing an ADC ligand to replace one isocyanide in these complexes increases their quantum yields significantly, with enhancements ranging from  $1.2\times$  to  $2.7\times$ , giving  $\Phi_{PL}$  values of 0.07 to 0.56 in 2a-e. When  $C^N=$  piq and pq and the PL occurs at the longest wavelengths in the series, the ADC brings about the smallest relative enhancements in photoluminescence quantum yields, at  $1.2\times$  for 1a/2a and  $1.4\times$  for 2a/2b, suggesting that the ADC has less of an impact on the photoluminescence quantum yields in the orange to red spectral regions. In contrast, for the higher-energy emitters in the blue to green regions (1c-e and 2c-e), much larger increases in  $\Phi_{PL}$  occur in the ADC compounds.

The photoluminescence (PL) lifetimes of all compounds fall within the microsecond range (10-68  $\mu$ s), strongly indicating PL from a triplet excited state. Concomitant with the large increases in  $\Phi_{PL}$ , for the ADC-modified complexes 2c-2ethere is also a notable increase in phosphorescence lifetime compared to the bis-isocyanide complexes 1c-1e. Significant decreases in the nonradiative decay rate constant,  $k_{nr}$ , contribute to the longer lifetimes and are likely due to the stronger  $\sigma$ -donor properties and ligand-field strength of the carbene ligands. As we have characterized previously in other classes of ADC-supported Pt(II) phosphors, 22,25,28 the nonradiative metal-centered d-d states (3MC) are destabilized in the ADC complexes, preventing their thermal population from the emissive T<sub>1</sub> state, and the data here are consistent with the same excited-state landscape. However, for complexes 2a and 2b, the phosphorescence lifetime is minimally altered or decreases slightly when compared to their isocyanide precursors 1a and 1b. The lifetime increases from 10 to 11  $\mu$ s when 1a is converted to 2a and decreases from 34 to 28  $\mu$ s when 1b is converted to 2b, again indicating that the ADC ligand has only a small influence on excited-state dynamics when the PL occurs in the lower-energy regions of the visible

The luminescence colors of all compounds can be more quantitatively evaluated using the Commission International de l'Eclairage (CIE) 1931 color coordinates, derived from photoluminescence data recorded in PMMA films at 2 wt %, as illustrated in Figure 6. Compounds with C^N = piq (1a and 2a) emit light in the red region, those with pq (1b and 2b) are in the orange region, ppy compounds (1c and 2c) fall within

Table 2. Summary of UV-vis Absorption and Photoluminescence Data

	UV-vis absorption <sup>a</sup>			Phot	toluminescence <sup>b</sup>		
Complex	$\lambda_{\mathrm{max}/\mathrm{nm}} \ (\varepsilon \times 10^{-3}/\mathrm{M}^{-1}\mathrm{cm}^{-1})$	$\lambda_{0-0}$ , $\lambda_{0-1}/\text{nm}$	$\Phi_{ ext{PL}}$	$\tau/\mu$ s	$k_{\rm r}/{ m s}^{-1}$	$k_{\rm nr}/{ m s}^{-1}$	(CIEx, CIEy)
1a	256 (52), 332 (13), 358 (9), 402 (5), 425 (3) (sh) <sup>c</sup>	601, 643	0.06	10	$6.0 \times 10^{3}$	$9.4 \times 10^{4}$	(0.62, 0.36)
1b	276 (46), 336 (13), 350 (14), 400 (4) (sh)	538, 574	0.27	34	$7.9 \times 10^{3}$	$2.1 \times 10^4$	(0.47, 0.52)
1c	275 (35), 316 (11), 332 (8), 364 (3) (sh)	480, 514	0.33	38	$8.7 \times 10^{3}$	$1.8 \times 10^{4}$	(0.25, 0.57)
1d	258 (32), 313 (13), 356 (3)	467, 499	0.21	37	$1.9 \times 10^{3}$	$2.5 \times 10^4$	(0.26, 0.44)
1e	265 (54), 299 (28), 339 (3) (sh)	434, 459	0.08	22	$3.6 \times 10^{3}$	$4.2 \times 10^4$	(0.17, 0.18)
2a	354 (12), 390 (6)	592, 630	0.07	11	$6.4 \times 10^{3}$	$8.5 \times 10^4$	(0.61, 0.38)
2b	278 (38), 334 (11), 352 (12), 402 (3) (sh)	536, 572	0.39	28	$1.4 \times 10^{4}$	$2.2 \times 10^4$	(0.47, 0.52)
2c	273 (27), 326 (8), 361 (3) (sh)	470, 503	0.50	56	$8.9 \times 10^{3}$	$8.9 \times 10^{3}$	(0.24, 0.47)
2d	256 (33), 320 (10), 360 (3) (sh)	454, 486	0.56	68	$4.3 \times 10^{3}$	$1.0 \times 10^{4}$	(0.19, 0.33)
2e	258 (42), 299 (12) (sh)	415, 440	0.15	31	$4.8 \times 10^{3}$	$2.7 \times 10^{4}$	(0.16, 0.11)

<sup>&</sup>quot;Recorded in CH<sub>2</sub>Cl<sub>2</sub> at room temperature. Brecorded at 2 wt % in PMMA films at room temperature. sh = shoulder.

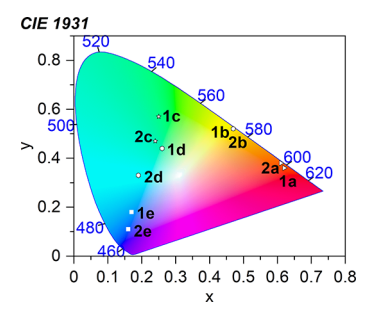


Figure 6. Chromaticity diagram showing the (CIEx, CIEy) coordinates of 1a-e and 2a-e recorded in PMMA films at 2 wt %.

the green region,  $F_2ppy$  analogues (1d and 2d) emit sky blue light, and ppz (1e and 2e) is associated with the blue region. In the same vein as their PL wavelengths, the CIE coordinates in blue to green-emitting 1c—e undergo larger shifts when the ADC is converted to an isocyanide, compared to orange and red-emitting 1a and 1b. Notably, complex 2e exhibits CIE coordinates that align with the criteria for deep blue luminescence, previously defined as CIEy < 0.15 and (CIEx + CIEy) < 0.30. Thus, the ADC has two beneficial impacts on the blue-phosphorescent analogues, shifting their color profiles deeper into the blue while simultaneously increasing the photoluminescence quantum yield, outcomes that are difficult to achieve together.

To investigate PL properties relevant to PhOLED devices (see below), we further examined the photoluminescence characteristics of high-performing bis-isocyanide and mono-ADC platinum complexes  $C^N = ppy$  (1c and 2c) and  $F_2ppy$ (1d and 2d) in spin-coated organic films. These complexes were doped at a higher concentration of 10 wt % into PMMA thin films and PVK:PBD (where PVK = poly(vinyl carbazole) and PBD = 2-(4-biphenyl)-5-(4-tert-butylphenyl)-1,3,4-oxadiazole) host matrix thin films using dichloromethane as the solvent for spin-coating. The overlaid PL spectra and chromaticity diagrams showing the (CIEx, CIEy) coordinates of these complexes in PMMA thin films at 10 wt % and PVK:PBD thin films at 10 wt % are depicted in Figures 7 and S44, respectively. Additionally, a summary of the photoluminescence properties of all sample films, including the  $\lambda_{0-0}$ values and PL quantum yields, is presented in Table 3. The results indicate that at the higher 10 wt % loading in PMMA, the  $\lambda_{0-0}$  values of all investigated compounds are nearly identical to those reported at 2 wt % loading. In PMMA at 10 wt %, the photoluminescence quantum yields of complexes 1c, 2c, 1d, and 2d are 0.32, 0.56, 0.21, and 0.56, respectively. The  $\Phi_{PL}$  values are similar at 2 and 10 wt % in PMMA, indicating no aggregation-caused quenching (ACQ) in this concentration range. However, in the PVK:PBD host matrix thin film containing these complexes at 10 wt %, the PL spectra reveal not only luminescence from the complexes themselves but also a shoulder peak originating from the PVK:PBD host matrix at 421 nm (Figure S44).

## **Electroluminescent Properties**

Despite several recent advances in ADC-supported platinum complexes reported by our group and others, which feature high photoluminescence quantum yields and lower non-radiative rate constants  $(k_{\rm nr})$ ,  $^{20,22,23,26}$  to date, there is limited insight on using ADC-supported platinum complexes for electrophosphorescent applications. Therefore, we fabricated identical PhOLED structures using compounds with C^N =

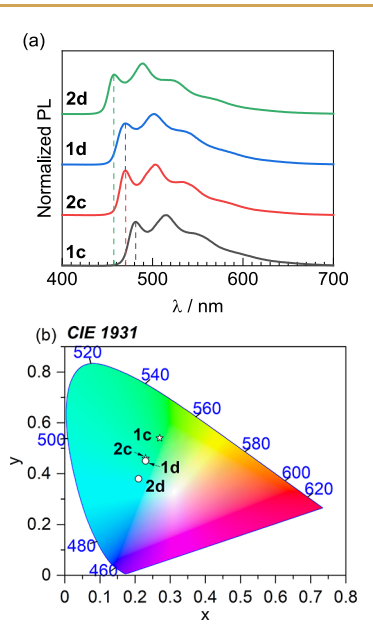


Figure 7. (a) The normalized PL spectra and (b) chromaticity diagram showing the (CIEx, CIEy) coordinates of compounds with  $C^N = \text{ppy (1c and 2c)}$  and  $F_2 \text{ppy (1d and 2d)}$  doped at 10 wt % PMMA in thin films.

Table 3. Photoluminescence Data of Compounds with  $C^N$  = ppy (1c and 2c) and  $F_2$ ppy (1d and 2d) Doped at 10 wt % in PMMA Thin Films and at 10 wt % in PVK:PBD Thin Films

	10 wt % in PMMA			10 wt % i	n PVK:PBD
Complex	$\lambda_{0-0}$ / nm	$\Phi_{ ext{PL}}$	(CIEx, CIEy)	$\lambda_{0-0}$ / nm	(CIEx, CIEy)
1c	482	0.32	(0.27, 0.54)	486	(0.29, 0.40)
2c	470	0.56	(0.23, 0.46)	473	(0.21, 0.27)
1d	470	0.21	(0.23, 0.45)	537 (max)	(0.30, 0.36)
2d	457	0.56	(0.21, 0.38)	464	(0.24, 0.39)

ppy (1c and 2c) and F<sub>2</sub>ppy (1d and 2d) as the emissive dopants, to investigate electroluminescence in this new class of complexes. The emissive layers of these devices contain 10 wt % of either bis-isocyanide Pt complexes (1c or 1d) or mono-ADC Pt complexes (2c or 2d), blended with a host matrix consisting of PVK for hole transport and PBD for electron transport. The complete PhOLED device architecture is illustrated in Figure 8a: indium tin oxide (ITO) (110 nm) serves as the anode, followed by a layer of poly(3,4ethylenedioxythiophene): poly(styrenesulfonate) (PE-DOT:PSS) (50 nm) as the hole injection layer (HIL). The emissive layer of 1c, 2c, 1d, or 2d (10 wt %):PVK:PBD (50 nm) was then deposited, followed by a layer of 2,2',2"-(1,3,5benzinetriyl)-tris(1-phenyl-1-H-benzimidazole) (TPBi) (40 nm) as the electron transport layer (ETL). The device was completed with a 100 nm layer of aluminum (Al) as the cathode. The chemical structures of all organic materials used in PhOLED fabrication are depicted in Figure S1.

The energy level diagram, *J-V* characteristics, electroluminescence (EL) spectra, and CIE chromaticity diagram of the PhOLED devices are presented in Figure 8 and Table 4. It is evident that the incorporation of ADCs into cyclometalated Pt complexes has a significant impact on the performance of the PhOLEDs. Figure 2 and Table 1 demonstrate that converting isocyanides into ADCs consistently widens the

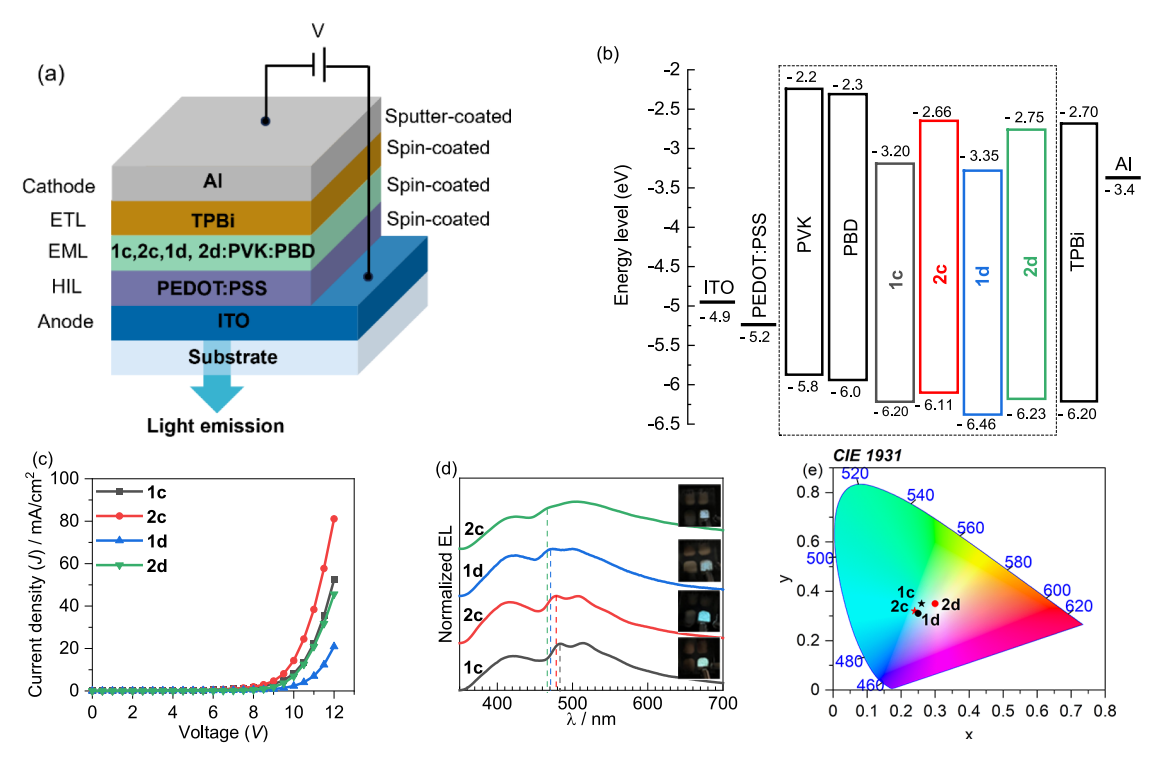


Figure 8. Device characteristics of PhOLEDs using compounds with  $C^N = ppy$  (1c and 2c) and  $F_2ppy$  (1d and 2d) as various emitters: (a) PhOLED device architecture, (b) Energy-level diagram of PhOLED devices illustrating HOMO and LUMO levels in eV, (c) Current density (*J*)-voltage (*V*) curves, (d) Electroluminescence spectra collected at an applied bias of 10 V with photographs in the inset and enlarged photographs in Figure S45, (e) chromaticity diagram showing the (CIEx, CIEy) coordinates of four PhOLEDs.

Table 4. Optoelectrical Performance of PhOLEDs Doped with Compounds with  $C^N = ppy$  (1c and 2c) and  $F_2ppy$  (1d and 2d) as the Emitters

Dopant	$J/mA cm^{-2aa}$	$\lambda_{\mathrm{EL,host}}, \lambda_{\mathrm{EL,0-0}}, \lambda_{\mathrm{EL,0-1/nm}}{}^{ab}$	(CIEx, CIEy)
1c	8.12	420, 485, 514 (max)	(0.26, 0.35)
2c	14.33	419, 479, 506 (max)	(0.24, 0.32)
1d	2.34	424, 471, 503 (max)	(0.25, 0.31)
2d	6.91	424, 466, 503 (max)	(0.30, 0.35)

"Values of current density (J) and  $\lambda_{\rm EL}$  were obtained at an applied bias of 10 V.  $^b\lambda_{\rm EL,host}$  is the peak wavelength for the PVK:PDB host in the PhOLED,  $\lambda_{\rm EL,0-0}$  is the dopant's phosphorescence 0–0 peak in the PhOLED, and  $\lambda_{\rm EL,0-1}$  is the dopant's 0–1 peak in the PhOLED, which is also the wavelength of maximum emission in all devices.

HOMO-LUMO gap, positioning the LUMO level of the ADC complexes (2c and 2d) near the LUMO of the TPBi ETL, as illustrated in Figure 8b. Consequently, PhOLEDs incorporating mono-ADC Pt complexes (2c and 2d) exhibit higher current density compared to those utilizing bisisocyanide Pt complexes (1c and 1d), as depicted in Figure 8c.

The PhOLEDs summarized in Figure 8 exhibit electroluminescence (EL) with peaks ( $\lambda_{0-0}$ ) at 485, 479, 471, and 466 nm with 1c, 2c, 1d, and 2d, as the dopant, respectively, similar to the photoluminescence (PL) of the complexes in PMMA or PVK:PDB thin films (Figure 7 and Table 3). However, in all PhOLED devices, a broad high-energy band is observed at around 420 nm, which is attributed to emission from the PVK host or a PBD:PVK exciplex, 35–37 as also seen in the PL spectra recorded in the same host (Figure S44). The CIE coordinates of the PhOLEDs are shown in Figure 8e. As a result of the broad host emission, the color profiles of all PhOLEDs are similar, and the devices containing 10 wt % 1c,

**2c**, and **1d** display sky-blue EL with CIE coordinates of (0.26, 0.35), (0.24, 0.32), and (0.25, 0.31), respectively. The PhOLED containing 10 wt % **2d** produces essentially whitelight EL with CIE coordinates of (0.30, 0.35).

# CONCLUSIONS

In conclusion, this study presents a comprehensive investigation into the synthesis, structural characterization, electrochemical behavior, and photophysical properties of luminescent cyclometalated platinum complexes supported by acyclic diaminocarbene (ADC) ligands. Through the integration of ADC donors with diverse C^N cyclometalating ligands, the study elucidates the collective effects on the photophysical properties of these complexes. Electrochemical studies reveal significant shifts in redox potentials and HOMO-LUMO gaps upon conversion of isocyanides into ADCs, highlighting the influence of the ADC on the frontier orbital energies. Photophysical investigations demonstrate modulation of the UV-vis absorption and PL spectra, with the ADC inducing a blue shift in PL and enhancing photoluminescence quantum yields, most profoundly in complexes which luminesce in the blue region. The observed increase in phosphorescence lifetimes for ADC-modified complexes underscores the role of ADC in minimizing nonradiative decay processes, thereby improving the overall luminescence efficiency. Solutionprocessed PhOLEDs employing mono-ADC Pt complexes with  $C^N = ppy$  or  $F_2ppy$  as the emitters were successfully fabricated and display sky-blue or white EL. Overall, these findings highlight the potential of ADC ligands in enhancing the photophysical properties of luminescent platinum complexes, with implications for optoelectronic applications. The study also contributes to the understanding of structureproperty relationships in luminescent platinum complexes and creates new paths for exploring how to design and develop advanced luminescent materials with specific optical properties.

#### EXPERIMENTAL SECTION

#### Materials

All synthesis reactions were performed in a nitrogen-filled glovebox. Starting materials and reagents were purchased from commercial sources and used without further purification unless otherwise specified. Dried and degassed solvents were obtained via a Grubbs Solvent Purification System. The precursors  $[Pt(C^N)(\mu-Cl)]_2$  were prepared with conventional heating, as previously described.<sup>38</sup>

## **Physical Methods**

<sup>1</sup>H, <sup>13</sup>C{<sup>1</sup>H}, and <sup>19</sup>F NMR spectra were recorded at room temperature using a JEOL ECA-400, NMR spectrometer. NMR was primarily used to validate bulk purity of the synthesized compounds. Elemental analysis, performed by Atlantic Microlab, confirmed the bulk purity of three complexes (1c, 2c, 1d) used as PhOLED dopants. The observed mass percents of carbon, hydrogen, and nitrogen for each complex are good matches for the theoretical values, as summarized in Table S5. Infrared (IR) spectra were obtained using a Thermo Nicolet Avatar FT-IR spectrometer with a diamond ATR. Cyclic voltammograms were recorded using a CH Instruments 602E potentiostat interfaced with a glovebox via wire feedthroughs. Samples were dissolved in MeCN with 0.1 M TBAPF<sub>6</sub> as the supporting electrolyte. A 3 mm diameter glassy carbon working electrode, a platinum wire counter electrode, and a silver wire pseudoreference electrode were used in each experiment. Potentials were referenced to an internal standard of ferrocene, which was added before recording the last in a series of voltammograms for a particular compound. Most of the redox couples are electrochemically irreversible, so the half-peak method recommended by Vullev et al.<sup>32</sup> Briefly, the CV data was plotted in Origin Pro and the peak anodic or cathodic current, relative to the baseline, was determined for each wave. Then, the wave was traced until the current reached half of the peak value, and the potential at which that occurred was recorded as the reduction potential for that event. UV-vis absorption spectra were recorded in dichloromethane in screw-capped 1 cm quartz cuvettes using an Agilent Cary 8454 UV-vis spectrophotometer. Steady-state photoluminescence (PL) and excitation spectra were recorded using a Horiba FluoroMax-4 spectrofluorometer. Air-free samples for PL spectra were prepared in a nitrogen-filled glovebox using dry, deoxygenated solvents. Room-temperature PL measurements in solution were housed in 1 cm quartz cuvettes with septum-sealed screw caps. The photoluminescence quantum yields  $(\Phi_{PL})$  of complexes doped at 2 or 10 wt % into poly(methyl methacrylate) (PMMA) or PVK:PDF thin films were recorded using a Spectralon-coated integrating sphere (150 mm diameter, Labsphere) exciting at 310, 320, 340, or 360 nm. The  $\Phi_{\text{PL}}$  value for each complex is reported as an average of independent measurements on three different samples. Phosphorescence lifetimes were measured on a Horiba DeltaFlex Lifetime System, using 330 or 360 nm excitation.

#### PMMA and PVK:PDB Thin Film Fabrication

To prepare PMMA films with 2 wt % of the platinum complex, inside a nitrogen-filled glovebox, 98 mg of PMMA (35 kDa) and 2 mg of platinum complex were dissolved in 1 mL of dichloromethane. The solution was then drop-coated onto a quartz substrate and dried at room temperature overnight prior to use.

The 10 wt % samples in PMMA thin film were spin-coated onto a quartz substrate at 2000 rpm for 20 s from a mixed dichloromethane solution (10 mg/mL) of PMMA and the respective Pt complex. Similarly, the 10 wt % Pt complex in PVK:PBD thin film (63 wt % PVF and 27 wt % PDB) was spin-coated onto a quartz substrate at 2000 rpm for 20 s from a mixed dichloromethane solution (10 mg/mL) of PVK:PBD and the Pt complex (see Figure S1 for the structures of PVK and PDB).

#### **PhOLED Fabrication and Testing**

The device was fabricated on commercially obtained glass substrates with a layer of indium tin oxide (ITO) and a sheet resistance of 20  $\Omega$  sq<sup>-1</sup>, purchased form Ossila Inc. The substrates were cleaned with acetone, acetone/ethanol and isopropanol in an ultrasonic bath for 15 min each, followed by treatment with UV ozone for 15 min to improve solution wetting. The PhOLED devices were fabricated with the following configuration: ITO (110 nm)/ PEDOT:PSS (50 nm)/1c, 2c, 1d, or 2d (10 wt %):PVK: PBD (50 nm)/TPBi (40 nm)/Al (100 nm)). The 1.7 wt % PEDOT:PSS (1:6 w/w) solution in water was filtered through using a 0.45  $\mu$ m hydrophilic filter. A PEDOT:PSS layer, approximately 50 nm thick, was then spin-coated (5000 rpm, 40 s) onto the ITO substrate and annealed at 130 °C for 30 min on a hot plate. Next the emissive layer, also 50 nm thick, was spin-coated (2000 rpm, 20 s) from a mixed dichloromethane solution (10 mg/mL) of PVK, PBD and the respective Pt complex. The TPBi was dispersed in ethanol at a concentration of 3 mg/mL through 30 min of sonication. The TPBi layer, 40 nm thick, was spin-coated (2000 rpm, 30 s) and subsequently annealed at 50 °C in a vacuum oven. Finally, a 100 nm layer of Al was deposited via sputter coating at a pressure of 10<sup>-6</sup> mbar. The electroluminescence spectra of the PhOLEDs were obtained using a Horiba FluoroMax-4 spectrofluorometer and a Keithley 2400 power source. Current density-voltage (J-V) characteristics were measured using a Keithley 2400 power source.

#### X-ray Crystallography Details

Single crystals were mounted on a Bruker Apex II three-circle diffractometer using Mo K $\alpha$  radiation ( $\lambda = 0.71073$  Å). All the data was collected at 123 or 298 K (1e only), then processed and refined within the APEXII software. Structures were solved by intrinsic phasing methods in SHELXT and refined by standard difference Fourier techniques in the program SHELX.<sup>39</sup> Hydrogen atoms bonded to carbon were placed in calculated positions using the standard riding model and refined isotropically; all non-hydrogen atoms were refined anisotropically. Hydrogen atoms bonded to nitrogen in complexes 2a-e were located in the difference map and refined isotropically, restraining the N-H bond distance to 0.88 Å and the hydrogen displacement parameter to 1.2× that of the N atom it is bonded to. In the structures of 1e, 2b, 2c, and 2d, disorder was observed in one or more locations of the main moieties, counterions, or solvent molecules. These include positional disorders of solvent molecules and rotational disorders of PF<sub>6</sub><sup>-</sup> counterions. All disordered parts were

restrained with distance restraints (SADI in SHELX) and rigid-bond restraints (SIMU and DELU in SHELX). The crystal of **2a** was found to be a nonmerohedral twin and was refined against two unit cell domains. Due to low crystal quality, the twinning was not completely resolved, leading to a level B checkCIF errors after refinement. As a result, the structural metrics (bond distances and bond lengths) in **2a** are not very reliable, but the final refined model does conclusively confirm the proposed molecular structure. All crystallographic details are summarized in Tables S1–S3.

## General Procedure for Bis-Isocyanide Complexes 1a-1e

A 100 mg amount of the dimer  $[Pt(C^N)(\mu-Cl)]_2$  was dissolved in 20 mL of dichloromethane, and 2.5 equiv of AgPF<sub>6</sub> and 5 equiv of 2,6-dimethylphenyl isocyanide  $(CN^{dmp})$  were added. The solution was stirred overnight at room temperature. After 1 day the solution was removed from the glovebox and filtered through Celite to remove the AgCl byproduct. The solution was then evaporated to around 2 mL and pentane or diethyl ether was added to form a precipitate. The precipitate was filtered and washed with pentane or diethyl ether, then dried under vacuum.

Preparation of [Pt(piq)(CN<sup>dmp</sup>)<sub>2</sub>](PF<sub>6</sub>) (1a). Prepared by the general procedure using  $[Pt(piq)(\mu-Cl)]_2$  (100 mg, 0.113 mmol), AgPF<sub>6</sub> (70 mg, 0.25 mmol), and 2,6-dimethylphenyl isocyanide (80 mg, 0.50 mmol). The product was purified by slow crystallization overnight from a dichloromethane solution layered with diethyl ether. Yield: 30% (55 mg, 0.068 mmol). H NMR (400 MHz, Acetonitrile-d<sub>3</sub>):  $\delta$  8.89 (d, I = 8.8 Hz, 1H, ArH), 8.82 (d, J = 6.3 Hz, 1H, ArH), 8.24 (d, J = 7.8 Hz, 1H, ArH), 8.06 (d, J = 8.1 Hz, 1H, ArH), 7.95 (t, J = 7.6 Hz, 1H, ArH), 7.84 (t, J = 7.3 Hz, 2H, ArH), 7.78 (d, J = 6.4 Hz, 1H, ArH), 7.45–7.32 (m, 4H, ArH), 7.30–7.26 (m, 4H, ArH), 2.50 (s, 12H,  $ArC_{\underline{H}_3}$ ). <sup>13</sup>C{<sup>1</sup>H} NMR: (101 MHz, Acetonitrile- $d_3$ )  $\delta$  169.0, 150.8, 148.4, 144.7, 138.7, 138.4, 136.5, 136.2, 133.8, 131.9, 131.3, 131.1 (d, *J* = 10.1 Hz), 131.0, 130.0, 128.5, 127.82, 127.75, 126.8, 125.4, 123.0, 18.1 (Ar<u>C</u>H<sub>3</sub>). FT-IR:  $\tilde{\nu}_{C=N} = 2179 \text{ cm}^{-1}$ .

Preparation of [Pt(pq)(CN<sup>dmp</sup>)<sub>2</sub>](PF<sub>6</sub>) (1b). Prepared by the general procedure using [Pt(pq)( $\mu$ -Cl)]<sub>2</sub> (100 mg, 0.113 mmol), AgPF<sub>6</sub> (70 mg, 0.25 mmol), and 2,6-dimethylphenyl isocyanide (80 mg, 0.50 mmol). Yield: 78% (143 mg, 0.177 mmol). <sup>1</sup>H NMR (400 MHz, Acetone-d<sub>6</sub>): δ 8.80 (d, J = 8.8 Hz, 1H, ArH), 8.66 (d, J = 8.8 Hz, 1H, ArH), 8.33 (d, J = 8.8 Hz, 1H, ArH), 8.12 (d, J = 8.1 Hz, 1H, ArH), 8.07–8.04 (m, 1H, ArH), 7.95–7.89 (m, 2H, ArH), 7.74 (t, J = 7.9 Hz, 1H, ArH), 7.47–7.33 (m, 6H, ArH), 7.25 (d, J = 7.7 Hz, 2H, ArH), 2.55 (s, 6H, ArCH<sub>3</sub>), 2.36 (s, 6H, ArCH<sub>3</sub>). <sup>13</sup>C{<sup>1</sup>H} NMR (101 MHz, Acetone-d<sub>6</sub>): δ 147.8, 146.9, 143.9, 138.0, 136.2, 132.8, 132.5, 131.19, 131.14, 129.8, 128.7, 128.6, 128.5, 128.2, 127.7, 127.33, 127.28, 118.0, 18.0 (ArCH<sub>3</sub>), 17.9 (ArCH<sub>3</sub>). FT-IR:  $\tilde{\nu}_{C\equiv N}$  = 2183 cm<sup>-1</sup>.

Preparation of [Pt(ppy)(CN<sup>dmp</sup>)<sub>2</sub>](PF<sub>6</sub>) (1c). Prepared by the general procedure using [Pt(ppy)( $\mu$ -Cl)]<sub>2</sub> (100 mg, 0.130 mmol), AgPF<sub>6</sub> (78 mg, 0.31 mmol), and 2,6-dimethylphenyl isocyanide (86 mg, 0.65 mmol). Yield: 83% (165 mg, 0.217 mmol). <sup>1</sup>H NMR (400 MHz, Acetonitrile-d<sub>3</sub>): δ 8.97 (d, J = 5.7 Hz, 1H, Ar $\underline{\text{H}}$ ), 8.17 (t, J = 7.8 Hz, 1H, Ar $\underline{\text{H}}$ ), 8.05 (d, J = 8.1 Hz, 1H, Ar $\underline{\text{H}}$ ), 7.81 (d, J = 6.1 Hz, 2H, Ar $\underline{\text{H}}$ ), 7.45-7.24 (m, 9H, Ar $\underline{\text{H}}$ )), 2.50 (s, 12H, ArC $\underline{\text{H}}$ <sub>3</sub>). <sup>13</sup>C{<sup>1</sup>H} NMR (101 MHz, Acetonitrile-d<sub>3</sub>): δ 166.7, 153.8, 150.0, 147.1, 142.5, 138.0, 136.5, 136.1, 131.8, 131.3, 130.9, 128.5, 128.4, 127.3,

125.25, 125.15, 120.7, 18.14 (Ar $\underline{C}$ H<sub>3</sub>), 18.07 (Ar $\underline{C}$ H<sub>3</sub>). FT-IR:  $\tilde{\nu}_{C\equiv N} = 2179 \text{ cm}^{-1}$ .

Preparation of [Pt(F<sub>2</sub>ppy)(CN<sup>dmp</sup>)<sub>2</sub>](PF<sub>6</sub>) (1d). Prepared by the general procedure using [Pt(F<sub>2</sub>ppy)( $\mu$ -Cl)]<sub>2</sub> (100 mg, 0.119 mmol), AgPF<sub>6</sub> (75 mg, 0.30 mmol), and 2,6-dimethylphenyl isocyanide (79 mg, 0.60 mmol). Yield: 55% (110 mg, 0.131 mmol). <sup>1</sup>H NMR (400 MHz, Acetonitrile-d<sub>3</sub>): δ (ppm) 9.01 (dd, J = 5.7, 1.3 Hz, 1H, ArH), 8.29–8.17 (m, 2H, ArH), 7.48–7.32 (m, 4H, ArH), 7.33–7.20 (m, 4H, ArH), 6.90 (ddd, J = 12.6, 9.1, 2.4 Hz, 1H, ArH), 2.50 (s, 6H, ArCH<sub>3</sub>), 2.46 (s, 6 H, ArCH<sub>3</sub>). <sup>19</sup>F NMR (376 MHz, Acetonitrile-d<sub>3</sub>): δ –72.83 (d,  $J_{P-F} = 707$  Hz, 6F, PE<sub>6</sub><sup>-</sup>), –106.79 (m, 1F, ArE), –108.13 (m, 1F, ArE). FT-IR:  $\tilde{\nu}_{C\equiv N} = 2179$  cm<sup>-1</sup>.

Preparation of [Pt(ppz)(CN<sup>dmp</sup>)<sub>2</sub>](PF<sub>6</sub>) (1e). Prepared by the general procedure using [Pt(F<sub>2</sub>ppy)( $\mu$ -Cl)]<sub>2</sub> (100 mg, 0.135 mmol), AgPF<sub>6</sub> (85 mg, 0.34 mmol), 2,6-dimethylphenyl isocyanide (89 mg, 0.68 mmol). Yield: 48% (102 mg, 0.129 mmol). <sup>1</sup>H NMR (500 MHz, Acetonitrile-d<sub>3</sub>): δ 8.37 (dd, J = 2.9, 0.6 Hz, 1H, ArH), 8.15 (dd, J = 2.4, 0.6 Hz, 1H, ArH), 7.94–7.68 (m, 1H, ArH), 7.56 (dd, J = 8.0, 0.9 Hz, 3H, ArH), 7.44–7.32 (m, 4H, ArH), 7.30–7.24 (m, 1H, ArH), 7.19 (td, J = 7.5, 1.2 Hz, 1H, ArH), 2.500 (s, 6H, ArCH<sub>3</sub>), 2.495 (s, 6H, Ar (s, 6H, ArCH<sub>3</sub>).  $^{13}$ C{ $^{1}$ H} NMR (101 MHz, Acetonitrile-d<sub>3</sub>): δ 144.6, 144.4, 138.4, 136.6, 136.3, 135.3, 131.3, 131.0, 129.9, 128.5, 127.9, 127.7, 113.1, 109.6, 18.09 (ArCH<sub>3</sub>), 18.07 (ArCH<sub>3</sub>). FT-IR:  $\tilde{\nu}_{C\equiv N}$  = 2187 cm<sup>-1</sup>.

## General Procedure for ADC Complexes 2a-2d

100 mg of the respective  $[Pt(C^N)(CN^{dmp})_2](PF_6)$  complex (1a-d) was dissolved in a minimum amount of dichloromethane, then about 6 mL of diethylamine was added. The solution was stirred for 2 days. After 2 days, a white solid had formed, which was removed by filtration. The filtrate was diluted with dichloromethane and extracted with water.  $MgSO_4$  was added to dry the organic layer, which was concentrated to about 2 mL. Then, pentane or diethyl ether was added to form a precipitate. The precipitate was washed with pentane or diethyl ether, the remaining volatiles removed under vacuum, and the resulting powder further dried under

Preparation of [Pt(piq)(ADC)(CN<sup>dmp</sup>)](PF<sub>6</sub>) (2a). Prepared by the general procedure using 1a (89 mg, 0.11 mmol). Yield: 30% (29 mg, 0.033 mmol). <sup>1</sup>H NMR (400 MHz, Acetonitrile- $d_3$ ):  $\delta$  8.84 (d, J = 8.7 Hz, 1H, ArH), 8.46 (d, J =6.4 Hz, 1H, Ar<u>H</u>), 8.16 (d, J = 7.7 Hz, 1H, Ar<u>H</u>), 8.04 (s,  $^{195}$ Pt satellites,  ${}^{3}J_{Pt-H} = 102 \text{ Hz}$ , 1H, NH), 7.95 (d, J = 8.2 Hz, 1H, ArH), 7.88 (t, J = 7.5 Hz, 1H, ArH), 7.79 (t, J = 7.6 Hz, 1H, ArH), 7.56-7.51 (m, 2H, ArH), 7.43-7.24 (m, 5H, ArH), 7.07 (t, J = 7.5 Hz, 1H, Ar $\underline{\text{H}}$ ), 6.93–6.83 (m, 2H, Ar $\underline{\text{H}}$ ), 4.63– 4.57 (m, 1H,  $NCH_2CH_3$ ), 3.88–3.69 (m, 3H,  $NCH_2CH_3$ ), 2.30 (s, 6H, ArCH<sub>3</sub>), 2.03 (s, 3H, ArCH<sub>3</sub>), 1.99 (s, 3H,  $ArCH_3$ ), 1.48 (t, J = 7.2 Hz, 3H,  $NCH_2CH_3$ ), 1.35 (t, J = 7.1Hz, 3H, NCH<sub>2</sub>CH<sub>3</sub>). <sup>13</sup>C{<sup>1</sup>H} NMR (101 MHz, Acetonitrile $d_3$ ):  $\delta$  178.3 (ADC), 167.6, 155.7, 148.8, 143.2, 138.0, 137.9, 137.1, 136.7, 136.4, 135.71, 132.7, 130.8, 130.6, 130.3, 129.5, 128.8, 128.6, 128.3, 128.0, 127.6, 127.5, 125.4, 122.4, 117.5, 53.3 (NCH<sub>2</sub>CH<sub>3</sub>), 42.5 (NCH<sub>2</sub>CH<sub>3</sub>), 19.0 (ArCH<sub>3</sub>), 18.2  $(Ar\underline{C}H_3)$ , 13.4  $(NCH_2\underline{C}H_3)$ , 11.7  $(NCH_2\underline{C}H_3)$ . FT-IR:  $\tilde{\nu}_{C\equiv N}$ = 2155 cm<sup>-1</sup>,  $\tilde{\nu}_{\rm N-H}$  = 3356 cm<sup>-1</sup>.

Preparation of [Pt(pq)(ADC)(CN<sup>dmp</sup>)](PF<sub>6</sub>) (2b). Prepared by the general procedure using 1b (112 mg, 0.138 mmol). Yield: 24% (29 mg, 0.033 mmol). <sup>1</sup>H NMR (400

MHz, Acetone-d<sub>6</sub>): δ 8.65 (d, J = 8.7 Hz, 1H, Ar $\underline{H}$ ), 8.27 (d, J = 8.8 Hz, 1H), 8.03–7.96 (m, 3H, Ar $\underline{H}$ ), 7.62–7.53 (m, 3H, Ar $\underline{H}$ ), 7.42–7.28 (m, 3H, Ar $\underline{H}$ ), 7.35 (s, 1H, N $\underline{H}$ ), 7.22 (d, J = 7.7 Hz, 2H, Ar $\underline{H}$ ), 7.16–7.06 (m, 2H, Ar $\underline{H}$ ), 6.94 (d, J = 7.1 Hz, 1H, Ar $\underline{H}$ ), 4.48–4.39 (m, 1H, NC $\underline{H}_2$ CH<sub>3</sub>), 4.20–3.93 (m, 3H, NC $\underline{H}_2$ CH<sub>3</sub>), 2.24 (s, 3H, ArC $\underline{H}_3$ ), 2.21 (s, 6H, ArC $\underline{H}_3$ ), 2.12 (s, 3H, ArC $\underline{H}_3$ ), 1.58 (t, J = 7.1 Hz, 3H, NCH<sub>2</sub>C $\underline{H}_3$ ), 1.33 (t, J = 7.1 Hz, 3H, NCH<sub>2</sub>C $\underline{H}_3$ ), 1.37 (I + NMR (101 MHz, Acetone-d<sub>6</sub>): δ 168.5 (ADC), 148.6, 147.0, 141.8, 136.9, 135.3, 131.4, 131.1, 130.4, 129.2, 128.9, 128.6, 128.2, 128.0, 127.5, 127.4, 126.3, 126.0, 117.72, 53.3 (N $\underline{C}$ H<sub>2</sub>CH<sub>3</sub>), 42.1 (N $\underline{C}$ H<sub>2</sub>CH<sub>3</sub>), 19.0 (Ar $\underline{C}$ H<sub>3</sub>), 18.8 (Ar $\underline{C}$ H<sub>3</sub>), 18.1 (Ar $\underline{C}$ H<sub>3</sub>), 13.0 (NCH<sub>2</sub>CH<sub>3</sub>), 12.1 (NCH<sub>2</sub>CH<sub>3</sub>). FT-IR:  $\tilde{\nu}_{C\equiv N}$  = 2156 cm<sup>-1</sup>,  $\tilde{\nu}_{N-H}$  = 3356 cm<sup>-1</sup>.

Preparation of [Pt(ppy)(ADC)(CN<sup>dmp</sup>)](PF<sub>6</sub>) (2c). Prepared by the general procedure using 1c (93 mg, 0.123 mmol). Yield: 33% (34 mg, 0.041 mmol). <sup>1</sup>H NMR (400 MHz, Acetonitrile-d<sub>3</sub>):  $\delta$  8.60 (d, J = 5.7 Hz, 1H, ArH), 8.07 (s, <sup>195</sup>Pt satellites,  ${}^{3}J_{Pt-H} = 104 \text{ Hz}, N_{\underline{H}}$ ), 8.03 (t,  $J = 8.0 \text{ Hz}, 1H, Ar_{\underline{H}}$ ),  $7.97(d, J = 8.0 \text{ Hz}, 1\text{H}, \text{ArH}), 7.76 (d, J = 7.6 \text{ Hz}, 1\text{H}, \text{Ar}\underline{\text{H}}),$ 7.48-7.21 (m, 7H, Ar<u>H</u>), 7.14 (t, J = 7.5 Hz, 1H, Ar<u>H</u>), 6.96 $(d, J = 7.5 \text{ Hz}, 1H, Ar\underline{H}), 6.90 (d, J = 7.5 \text{ Hz}, 1H, Ar\underline{H}), 4.56$ (m, 1H,  $NCH_2CH_3$ ), 3.93–3.68 (m, 3H,  $NCH_2CH_3$ ), 2.32 (s, 6H,  $ArCH_3$ , 2.00 (s, 6H,  $ArCH_3$ ), 1.49 (t, J = 7.2 Hz, 3H,  $NCH_2CH_3$ ), 1.35 (t, J = 7.1 Hz, 3H,  $NCH_2CH_3$ )  $^{13}C\{^1H\}$ NMR (101 MHz, Acetonitrile- $d_3$ ):  $\delta$  178.2 (ADC), 154.9, 151.8, 140.7, 138.0, 137.1, 136.7, 136.3, 135.7, 130.7, 130.5, 128.9, 128.5, 128.4, 128.1, 126.1, 124.7, 124.3, 120.2, 53.3  $(NCH_2CH_3)$ , 42.5  $(NCH_2CH_3)$ , 18.9  $(ArCH_3)$ , 18.21 (Ar<u>C</u>H<sub>3</sub>), 18.18 (Ar<u>C</u>H<sub>3</sub>), 13.2 (NCH<sub>2</sub><u>C</u>H<sub>3</sub>), 11.7 (NCH<sub>2</sub><u>C</u>H<sub>3</sub>). FT-IR:  $\tilde{\nu}_{\text{C}\equiv\text{N}} = 2168 \text{ cm}^{-1}$ ,  $\tilde{\nu}_{\text{N}}_{\text{H}} = 3356 \text{ cm}^{-1}$ .

Preparation of [Pt(F<sub>2</sub>ppy)(ADC)(CN<sup>dmp</sup>)](PF<sub>6</sub>) (2d). Prepared by the general procedure using 1d (100 mg, 0.126 mmol). Yield: 31% (34 mg, 0.039 mmol). <sup>1</sup>H NMR (500 MHz, Acetonitrile-d<sub>3</sub>): δ 8.70–8.59 (m, 1H, Ar $\underline{H}$ ), 8.20 (d, J = 8.5 Hz, 1H, Ar $\underline{H}$ ), 8.10 (s, 1H, N $\underline{H}$ ), 8.05 (t, J = 8.2 Hz, 1H, Ar $\underline{H}$ ), 7.41 (t, J = 7.8 Hz, 1H, Ar $\underline{H}$ ), 7.29–7.21 (m, 3H, Ar $\underline{H}$ ), 7.13 (t, J = 7.5 Hz, 1H, Ar $\underline{H}$ ), 7.05–6.90 (m, 2H, Ar $\underline{H}$ ), 6.89–6.77 (m, 2H, Ar $\underline{H}$ ), 4.53–4.44 (m, 1H, NC $\underline{H}$ <sub>2</sub>CH<sub>3</sub>), 3.91–3.68 (m, 3H, NC $\underline{H}$ <sub>2</sub>CH<sub>3</sub>), 1.99 (s, 3H, ArC $\underline{H}$ <sub>3</sub>), 1.47 (t, J = 7.2 Hz, 3H, NCH<sub>2</sub>C $\underline{H}$ <sub>3</sub>), 1.33 (t, J = 7.1 Hz, 3H, NCH<sub>2</sub>C $\underline{H}$ <sub>3</sub>). <sup>19</sup>F NMR (376 MHz, Acetonitrile-d<sub>3</sub>): δ –72.84 (d, J<sub>P-F</sub> = 707 Hz, 6F, P $\underline{F}$ <sub>6</sub><sup>-</sup>), –108.73 (m, 1F, Ar $\underline{F}$ ), –109.36 (m, 1F, Ar $\underline{F}$ ). FT-IR:  $\tilde{\nu}$ <sub>C=N</sub> = 2172 cm<sup>-1</sup>,  $\tilde{\nu}$ <sub>N-H</sub> = 3356 cm<sup>-1</sup>.

Preparation of  $[Pt(ppz)(ADC)(CN^{dmp})](PF_6)$  (2e). This compound was prepared by a slightly different procedure than what was used for 2a-d. Complex 1e (100 mg, 0.134 mmol) was dissolved in a minimum amount of THF, then about 6 mL of diethyl amine was added. The solution was refluxed and stirred for 2 days. After 2 days, a white solid had formed. The solid was filtered off, washed with diethyl ether and pentane, and dried under vacuum. Yield: 36% (40 mg, 0.048 mmol). <sup>1</sup>H NMR (400 MHz, Acetonitrile-d<sub>3</sub>):  $\delta$  8.25 (d, J = 2.8 Hz, 1H, ArH), 8.02 (s,  $^{195}$ Pt satellites,  $^{3}J_{\text{Pt-H}} = 100$  Hz, N<u>H</u> 1H), 7.71 (d, J = 2.3 Hz, 1H, ArH), 7.48–7.35 (m, 3H, ArH), 7.30–7.23 (m, 2H, ArH), 7.20 (dd, J = 7.4, 1.3 Hz, 1H, ArH), 7.12 (d, J =7.5 Hz, 1H, ArH), 6.95 (d, J = 7.6 Hz, 1H, ArH), 6.87 (d, J =7.6 Hz, 1H, ArH), 6.53 (t, J = 2.6 Hz, 1H, ArH), 4.53–4.43 (m, 1H,  $NCH_2CH_3$ ), 3.89–3.78 (m, 1H,  $NCH_2CH_3$ ), 3.76– 3.64 (m, 2H, NCH2CH3), 1.99 (s, 3H, ArCH3), 1.97 (s, 3H,  $ArCH_3$ ), 1.46 (t, J = 7.2 Hz, 3H,  $NCH_2CH_3$ ), 1.30 (t, J = 7.1Hz, 3H,  $NCH_2CH_3$ ). <sup>13</sup>C{<sup>1</sup>H} NMR (101 MHz, Acetone-d<sub>6</sub>):

 $\delta$  177.3 (ADC), 145.3, 142.6, 139.8, 138.3, 137.0, 136.1, 135.6, 130.6, 129.0, 128.6, 128.3, 128.0, 126.9, 126.7, 112.5, 109.1, 53.3 (NCH<sub>2</sub>CH<sub>3</sub>), 42.5 (NCH<sub>2</sub>CH<sub>3</sub>), 18.9 (ArCH<sub>3</sub>), 18.1 (ArCH<sub>3</sub>), 13.5 (NCH<sub>2</sub>CH<sub>3</sub>), 12.0 (NCH<sub>2</sub>CH<sub>3</sub>). FT-IR:  $\tilde{\nu}_{\text{C}\equiv\text{N}}$  = 2171 cm<sup>-1</sup>,  $\tilde{\nu}_{\text{N}-\text{H}}$  = 3363 cm<sup>-1</sup>.

## ASSOCIATED CONTENT

## **Supporting Information**

The Supporting Information is available free of charge at https://pubs.acs.org/doi/10.1021/acsaom.4c00347.

Chemical structures of PhOLED materials, X-ray crystallography summary tables, NMR spectra, IR spectra, additional X-ray crystal structures, additional photoluminescence data (PDF)

X-ray crystallographic data for complexes 1a, 1b, 1c, 1e, and 2ae (CIF)

#### **Accession Codes**

CCDC 2366334–2366342 contain the supplementary crystallographic data for this paper. These data can be obtained free of charge via <a href="www.ccdc.cam.ac.uk/data\_request/cif.">www.ccdc.cam.ac.uk/data\_request/cif.</a>, or by emailing <a href="mailto:data\_request@ccdc.cam.ac.uk">data\_request/cif.</a>, or by contacting The Cambridge Crystallographic Data Centre, 12 Union Road, Cambridge CB2 1EZ, UK; fax: + 44 1223 336 033.

## AUTHOR INFORMATION

## **Corresponding Author**

Thomas S. Teets — Department of Chemistry, University of Houston, Houston, Texas 77204-5003, United States;
orcid.org/0000-0002-7471-8467; Email: tteets@uh.edu

#### **Authors**

Yennie H. Nguyen – Department of Chemistry, University of Houston, Houston, Texas 77204-5003, United States;
ocid.org/0000-0002-4474-6176

Linh T. M. Dang – Department of Chemistry, University of Houston, Houston, Texas 77204-5003, United States

Marjolaine Cornu – Department of Chemistry, University of Houston, Houston, Texas 77204-5003, United States

Chenggang Jiang — Department of Chemistry, University of Houston, Houston, Texas 77204-5003, United States; orcid.org/0000-0002-2240-831X

Allana C. Darrow – Department of Chemistry, University of Houston, Houston, Texas 77204-5003, United States

Vinh Q. Dang — Department of Chemistry, University of Houston, Houston, Texas 77204-5003, United States; orcid.org/0000-0002-7081-227X

Complete contact information is available at: https://pubs.acs.org/10.1021/acsaom.4c00347

## **Author Contributions**

<sup>#</sup>Y.H.N., L.T.M.D., and M.C. contributed equally. The manuscript was written through contributions of all authors. All authors have given approval to the final version of the manuscript.

#### **Notes**

The authors declare no competing financial interest.

#### ACKNOWLEDGMENTS

We acknowledge the Welch Foundation (Grant number E-1887) and the National Science Foundation (Grant number CHE-1846831) for supporting this work.

#### REFERENCES

- (1) Hong, G.; Gan, X.; Leonhardt, C.; Zhang, Z.; Seibert, J.; Busch, J. M.; Bräse, S. A Brief History of OLEDs—Emitter Development and Industry Milestones. *Adv. Mater.* **2021**, *33* (9), 2005630.
- (2) Baldo, M. A.; O'Brien, D. F.; Thompson, M. E.; Forrest, S. R. Excitonic Singlet-Triplet Ratio in a Semiconducting Organic Thin Film. *Phys. Rev. B* **1999**, *60* (20), 14422–14428.
- (3) Siddiqui, I.; Kumar, S.; Tsai, Y.-F.; Gautam, P.; Shahnawaz; Kesavan, K.; Lin, J.-T.; Khai, L.; Chou, K.-H.; Choudhury, A.; Grigalevicius, S.; Jou, J.-H. Status and Challenges of Blue OLEDs: A Review. *Nanomaterials* **2023**, *13* (18), 2521.
- (4) Woo, J. Y.; Park, M.; Jeong, S.; Kim, Y.; Kim, B.; Lee, T.; Han, T. Advances in Solution-Processed OLEDs and Their Prospects for Use in Displays. *Adv. Mater.* **2023**, 35 (43), 2207454.
- (5) Park, H.; Ameen, S.; Kumaresan, R.; Lee, J.; Park, J.; Song, D.; Lee, J.; Heo, Y.; Kim, B.; Jin, S. Highly Efficient and Stable Green Phosphorescent Light-Emitting Diodes Based on Solution-Processable Ir(III) Complexes with Electron-Transporting Ancillary Ligands. *Adv. Opt. Mater.* 2023, 11 (9), 2202641.
- (6) Kumaresan, R.; Park, H.; Maheshwaran, A.; Park, H.; Do, Y.; Song, M.; Yoon, J.; Ahn, S. I.; Jin, S. High Performance Solution-Processed Deep-Blue Phosphorescence Organic Light-Emitting Diodes with EQE Over 24% by Employing New Carbenic Ir(III) Complexes. *Adv. Opt. Mater.* **2022**, *10* (2), 2101686.
- (7) He, R.; Domingues, R. A.; Valandro, S.; Schanze, K. S. Platinum Poly-Yne Featuring N-Heterocyclic Carbene Ligands: Synthesis, Properties, and Organic Light-Emitting Diode Application. *Macromolecules* **2021**, 54 (21), 9888–9895.
- (8) Huo, S.; Carroll, J.; Vezzu, D. A. K. Design, Synthesis, and Applications of Highly Phosphorescent Cyclometalated Platinum Complexes. *Asian J. Org. Chem.* **2015**, 4 (11), 1210–1245.
- (9) Kalinowski, J.; Fattori, V.; Cocchi, M.; Williams, J. A. G. Light-Emitting Devices Based on Organometallic Platinum Complexes as Emitters. *Coord. Chem. Rev.* **2011**, 255 (21–22), 2401–2425.
- (10) Garethwilliams, J.; Develay, S.; Rochester, D.; Murphy, L. Optimising the Luminescence of Platinum(II) Complexes and Their Application in Organic Light Emitting Devices (OLEDs). *Coord. Chem. Rev.* **2008**, 252 (23–24), 2596–2611.
- (11) Yoshida, M.; Kato, M. Cation-Controlled Luminescence Behavior of Anionic Cyclometalated Platinum(II) Complexes. Coord. Chem. Rev. 2020, 408, 213194.
- (12) Amouri, H. Luminescent Complexes of Platinum, Iridium, and Coinage Metals Containing *N*-Heterocyclic Carbene Ligands: Design, Structural Diversity, and Photophysical Properties. *Chem. Rev.* **2023**, 123 (1), 230–270.
- (13) Zhang, Q.-C.; Xiao, H.; Zhang, X.; Xu, L.-J.; Chen, Z.-N. Luminescent Oligonuclear Metal Complexes and the Use in Organic Light-Emitting Diodes. *Coord. Chem. Rev.* **2019**, 378, 121–133.
- (14) Kashina, M. V.; Luzyanin, K. V.; Dar'in, D. V.; Bezzubov, S. I.; Kinzhalov, M. A. Phosphorescent Cyclometalated Palladium(II) and Platinum(II) Complexes Derived from Diaminocarbene Precursors. *Inorg. Chem.* **2024**, *63* (12), 5315–5319.
- (15) Brooks, J.; Babayan, Y.; Lamansky, S.; Djurovich, P. I.; Tsyba, I.; Bau, R.; Thompson, M. E. Synthesis and Characterization of Phosphorescent Cyclometalated Platinum Complexes. *Inorg. Chem.* **2002**, *41* (12), 3055–3066.
- (16) Martínez-Junquera, M.; Lara, R.; Lalinde, E.; Moreno, M. T. Isomerism, Aggregation-Induced Emission and Mechanochromism of Isocyanide Cycloplatinated(II) Complexes. *J. Mater. Chem. C* **2020**, 8 (21), 7221–7233.
- (17) Katkova, S. A.; Luzyanin, K. V.; Novikov, A. S.; Kinzhalov, M. A. Modulation of Luminescence Properties for [Cyclometalated]-Pt<sup>II</sup>(Isocyanide) Complexes upon Co-Crystallisation with Halosub-

- stituted Perfluorinated Arenes. New J. Chem. 2021, 45 (6), 2948-2952.
- (18) Katkova, S. A.; Mikherdov, A. S.; Sokolova, E. V.; Novikov, A. S.; Starova, G. L.; Kinzhalov, M. A. Intermolecular (Isocyano Group)... $Pt^{II}$  Interactions Involving Coordinated Isocyanides in Cyclometalated  $Pt^{II}$  Complexes. *J. Mol. Struct.* **2022**, *1253*, 132230.
- (19) Sokolova, E. V.; Kinzhalov, M. A.; Smirnov, A. S.; Cheranyova, A. M.; Ivanov, D. M.; Kukushkin, V. Y.; Bokach, N. A. Polymorph-Dependent Phosphorescence of Cyclometalated Platinum(II) Complexes and Its Relation to Non-Covalent Interactions. *ACS Omega* **2022**, *7* (38), 34454–34462.
- (20) Martínez-Junquera, M.; Lalinde, E.; Moreno, M. T.; Alfaro-Arnedo, E.; López, I. P.; Larráyoz, I. M.; Pichel, J. G. Luminescent Cyclometalated Platinum(II) Complexes with Acyclic Diaminocarbene Ligands: Structural, Photophysical and Biological Properties. *Dalton Trans.* **2021**, *50* (13), 4539–4554.
- (21) Katkova, S. A.; Kozina, D. O.; Kisel, K. S.; Sandzhieva, M. A.; Tarvanen, D. A.; Makarov, S. V.; Porsev, V. V.; Tunik, S. P.; Kinzhalov, M. A. Cyclometalated Platinum(II) Complexes with Acyclic Diaminocarbene Ligands for OLED Application. *Dalton Trans.* **2023**, *52* (14), 4595–4605.
- (22) Wu, Y.; Wen, Z.; Wu, J. I.; Teets, T. S. Efficient Deep Blue Platinum Acetylide Phosphors with Acyclic Diaminocarbene Ligands. *Chem. Eur. J.* **2020**, *26* (68), 16028–16035.
- (23) Nguyen, Y. H.; Soares, J. V.; Nguyen, S. H.; Wu, Y.; Wu, J. I.; Teets, T. S. Platinum(II)-Substituted Phenylacetylide Complexes Supported by Acyclic Diaminocarbene Ligands. *Inorg. Chem.* **2022**, *61* (22), 8498–8508.
- (24) López-López, J. C.; Nguyen, Y. H.; Jiang, C.; Teets, T. S. Luminescent Platinum Complexes with  $\pi$ -Extended Aryl Acetylide Ligands Supported by Isocyanides or Acyclic Diaminocarbenes. *Inorg. Chem.* **2023**, 62 (43), 17843–17850.
- (25) Nguyen, Y. H.; Dang, V. Q.; Soares, J. V.; Wu, J. I.; Teets, T. S. Efficient Blue-Phosphorescent *trans*-Bis(Acyclic Diaminocarbene) Platinum(II) Acetylide Complexes. *Chem. Sci.* **2023**, *14* (18), 4857–4862.
- (26) Nguyen, Y. H.; Wu, Y.; Dang, V. Q.; Jiang, C.; Teets, T. S. Combined Nucleophilic and Electrophilic Functionalization to Optimize Blue Phosphorescence in Cyclometalated Platinum Complexes. J. Am. Chem. Soc. 2024, 146 (13), 9224–9229.
- (27) Na, H.; Teets, T. S. Highly Luminescent Cyclometalated Iridium Complexes Generated by Nucleophilic Addition to Coordinated Isocyanides. *J. Am. Chem. Soc.* **2018**, *140* (20), 6353–6360.
- (28) Na, H.; Cañada, L. M.; Wen, Z.; I-Chia Wu, J.; Teets, T. S. Mixed-Carbene Cyclometalated Iridium Complexes with Saturated Blue Luminescence. *Chem. Sci.* **2019**, *10* (25), *6*254–*6*260.
- (29) Kinzhalov, M. A.; Eremina, A. A.; Smirnov, A. S.; Suslonov, V. V.; Kukushkin, V. Y.; Luzyanin, K. V. Cleavage of Acyclic Diaminocarbene Ligands at an Iridium(III) Center. Recognition of a New Reactivity Mode for Carbene Ligands. *Dalton Trans.* **2019**, 48 (22), 7571–7582.
- (30) Kinzhalov, M. A.; Grachova, E. V.; Luzyanin, K. V. Tuning the Luminescence of Transition Metal Complexes with Acyclic Diaminocarbene Ligands. *Inorg. Chem. Front.* **2022**, *9* (3), 417–439.
- (31) Sutton, G. D.; Olumba, M. E.; Nguyen, Y. H.; Teets, T. S. The Diverse Functions of Isocyanides in Phosphorescent Metal Complexes. *Dalton Trans.* **2021**, *50* (48), 17851–17863.
- (32) Espinoza, E. M.; Clark, J. A.; Soliman, J.; Derr, J. B.; Morales, M.; Vullev, V. I. Practical Aspects of Cyclic Voltammetry: How to Estimate Reduction Potentials When Irreversibility Prevails. *J. Electrochem. Soc.* **2019**, *166* (5), H3175–H3187.
- (33) Chen, L.; Doeven, E. H.; Wilson, D. J. D.; Kerr, E.; Hayne, D. J.; Hogan, C. F.; Yang, W.; Pham, T. T.; Francis, P. S. Co-Reactant Electrogenerated Chemiluminescence of Iridium(III) Complexes Containing an Acetylacetonate Ligand. *ChemElectrochem* **2017**, 4 (7), 1797–1808.
- (34) Djurovich, P. I.; Mayo, E. I.; Forrest, S. R.; Thompson, M. E. Measurement of the Lowest Unoccupied Molecular Orbital Energies

- of Molecular Organic Semiconductors. *Org. Electron.* **2009**, *10* (3), 515–520.
- (35) Jiang, X.; Register, R. A.; Killeen, K. A.; Thompson, M. E.; Pschenitzka, F.; Hebner, T. R.; Sturm, J. C. Effect of Carbazole—Oxadiazole Excited-State Complexes on the Efficiency of Dye-Doped Light-Emitting Diodes. *J. Appl. Phys.* **2002**, *91* (10), 6717–6724.
- (36) Giovanella, U.; Botta, C.; Papagni, A.; Tubino, R.; Miozzo, L. Electroluminescence from Two Fluorinated Organic Emitters Embedded in Polyvinylcarbazole. *Appl. Phys. Lett.* **2005**, 87 (17), 171910.
- (37) Germino, J. C.; De Freitas, J. N.; Domingues, R. A.; Quites, F. J.; Faleiros, M. M.; Atvars, T. D. Z. Organic Light-Emitting Diodes Based on PVK and Zn(II) Salicylidene Composites. *Synth. Met.* **2018**, 241, 7–16.
- (38) Godbert, N.; Pugliese, T.; Aiello, I.; Bellusci, A.; Crispini, A.; Ghedini, M. Efficient, Ultrafast, Microwave-Assisted Syntheses of Cycloplatinated Complexes. *Eur. J. Inorg. Chem.* **2007**, 2007 (32), 5105–5111.
- (39) Sheldrick, G. M. Crystal Structure Refinement with SHELXL. Acta Crystallogr., Sect. C: struct. Chem. 2015, 71 (1), 3–8.